

DOI: 10.1002/adem.201500520

# Micro-Mechanical Behavior of an Exceptionally Strong Metal Matrix Nanocomposite Processed by High-Pressure Torsion\*\*

By Byungmin Ahn, Han-Joo Lee, In-Chul Choi, Megumi Kawasaki,\* Jae-Il Jang\* and Terence G. Langdon

*This research describes the micro-mechanical behavior of an Al–Mg alloy system synthesized from two separate commercial Al-1050 and ZK60 alloys through the application of high-pressure torsion (HPT) for five turns at room temperature. The essential mechanical characteristics of the alloys are observed at the corresponding phases in a multi-layered structure at the disk center but the edge contains a metal matrix nanocomposite (MMNC) exhibiting an apparent plastic instability and decreasing strain rate sensitivity under strain rates of  $10^{-4}$ – $10^{-3}$  s $^{-1}$ . The results demonstrate a significant opportunity for using HPT processing to prepare new alloy systems involving a wide range of MMNCs.*

## 1. Introduction

The processing of engineering metals through the application of severe plastic deformation (SPD) has attracted much attention for the production of ultrafine-grained (UFG) and

nanostructured metals.<sup>[1]</sup> Among the SPD techniques, high-pressure torsion (HPT) provides the potential for achieving true nanometer grains by processing a metal disk under a high compressive pressure and concurrent torsional straining.<sup>[2]</sup> A wide range of materials has been used for HPT processing and numerous reports are now available demonstrating an enhancement of the physical and mechanical characteristics through significant grain refinement and the intensive introduction of defects.<sup>[2,3]</sup>

Both aluminum and magnesium are widely used as light-weight structural metals having excellent physico-chemical and mechanical properties and with good strength/weight ratios in the finished products. Nevertheless, the fabrication of high-strength metals generally involves long-term processing conducted under extreme conditions using special facilities. Accordingly, processing by HPT was extended recently as a powder consolidation technique in mechanical alloying for fabricating dissimilar metallic systems based on Al and Mg; for example, Al–Fe,<sup>[4]</sup> Al–Mg,<sup>[5]</sup> Al–Ni,<sup>[6]</sup> Al–Ti,<sup>[7]</sup> Al–W,<sup>[8,9]</sup> and Mg–Zn–Y.<sup>[10]</sup> Nevertheless, there are practical difficulties associated with powder processing because of the requirements of high temperatures<sup>[6,7,9,10]</sup> or the use of a two-step process of cold/hot compaction prior to HPT consolidation<sup>[8]</sup> and the consequent inherent damage that may be imparted to the HPT anvils because of the stacking of fine hard powders in the depressions on the anvil surfaces.

The present study was undertaken specifically to explore the possibility of avoiding these difficulties by achieving direct diffusion bonding of Al and Mg disks through the HPT processing. To date, a single report showed a solid-state reaction in an Al–Cu system through the bonding of semicircular disks

[\*] Dr. M. Kawasaki, Dr. J.-I. Jang, H.-J. Lee  
Division of Materials Science and Engineering, Hanyang University, Seoul 133-791, South Korea  
E-mail: megumi@hanyang.ac.kr, jijang@hanyang.ac.kr  
Dr. B. Ahn

Departments of Energy Systems Research and Materials Science and Engineering, Ajou University, Suwon 443-749, South Korea

Dr. I.-C. Choi  
Institute for Applied Materials, Karlsruhe Institute of Technology, Karlsruhe 76344, Germany

Dr. M. Kawasaki, Dr. T. G. Langdon  
Departments of Aerospace and Mechanical Engineering and Materials Science, University of Southern California, Los Angeles, California 90089-1453, USA

Dr. T. G. Langdon  
Materials Research Group, Faculty of Engineering and the Environment, University of Southampton, Southampton SO17 1BJ, UK

[\*\*] This work was supported by the NRF Korea funded by MoE under Grant No. NRF-2014R1A1A2057697 (MK); the NRF Korea funded by MSIP under Grant No. NRF-2015R1A2A2A01002387 (BA); the NRF Korea funded by MSIP under Grant No. NRF-2013R1A1A2A10058551 (JII); and the European Research Council under ERC Grant Agreement No. 267464-SPDMETALS (TGL).

of Al and Cu through HPT at ambient temperature for up to 100 turns<sup>[11]</sup> and the procedure provided the potential for *architecturing* nanostructured materials by using conventional SPD processing techniques.<sup>[12]</sup> Accordingly, very recent reports demonstrated, for the first time, the synthesis of a multi-layered Al–Mg system through the bonding of separate Al and Mg disks by applying conventional HPT processing.<sup>[13,14]</sup> These earlier reports confirmed the feasibility of achieving a high hardness by estimating the accelerated diffusivity of Mg and Al due to the torsional pressure and by calculating the separate sums of the Hall–Petch strengthening, precipitation hardening, and solution strengthening. Moreover, the rapid diffusion of Mg atoms in the Al matrix was estimated under compression where this was occurring due to the severely deformed microstructure including the excess of vacancy-type defects introduced by HPT processing.<sup>[14]</sup> The estimated value was in excellent agreement with the calculated diffusivity for diffusion bonding of the Al and Mg phases and the activation energy for the formation of intermetallic nanolayers in the processed Al–Mg alloy system.

Accordingly, the present study was initiated to initially re-examine these new findings in the next section and then to provide, in the following sections, a detailed study of the micro-mechanical behavior of the Al–Mg alloy and to critically evaluate the feasibility of using HPT processing to synthesize new metal systems.

## 2. Synthesis of a Metal Matrix Nanocomposite Processed by High-Pressure Torsion

A very recent study demonstrated the formation of a multi-layered Al–Mg system through the bonding of separate Al and Mg disks and ultimately the rapid synthesis of an extra hard metal matrix nanocomposite through conventional HPT processing at room temperature.<sup>[13,14]</sup> A schematic illustration of the HPT processing is shown in Figure 1 where separate disks of a commercial-purity Al-1050 aluminum alloy and a ZK60 magnesium alloy were placed in the depression on the lower anvil of an HPT facility in the order of Al/Mg/Al and the stacked three disks were then processed by HPT under a pressure of 6.0 GPa for up to 10 revolutions using a rotation speed of 1 rpm under quasi-constrained conditions.<sup>[15]</sup> Each disk sample had a diameter of 10 mm and a thickness of  $\approx 0.83$  mm as described earlier<sup>[13,14]</sup> and they were stacked

without any glue or metal brushing treatment. It should be noted that the initial microstructures include coarse grain sizes of  $\approx 0.2$  mm in the Al-1050 alloy and bi-modal grain size distributions with coarse grains of  $\approx 25$   $\mu\text{m}$  with finer grain sizes of 4–5  $\mu\text{m}$  in the ZK60 alloy.

The microstructural results are shown in Figure 2a representing an overview taken by optical microscopy on the cross-sectional planes of the Al–Mg disks after HPT for, from the top, 1, 5, and 10 turns. In all micrographs, the bright regions denote the Al-rich phase and the dark regions correspond to the Mg-rich phase. Although the multi-layered structure with fragmented Mg layers was retained throughout the disk after one turn and the central regions of the disks after 5 and 10 turns, the disk peripheries at radii,  $r$ , greater than  $\approx 2.5$ –3.0 mm after five turns showed homogeneously distributed very fine Mg phases with thicknesses of  $\approx 150$  nm to 10  $\mu\text{m}$  confined within an Al matrix and the Mg phase was not visible at the disk edge at  $\approx 3 < r < 5$  mm after 10 turns.

Detailed microstructural analysis showed that a true nanostructure was formed with grain sizes of  $\approx 190$  nm and  $\approx 90$  nm at the disk edges after 5 and 10 turns, respectively, where the observed TEM micrographs are shown in Figure 2 for the disk edges of (b) five turns, and (c) 10 turns.<sup>[13]</sup> A detailed chemical analysis by energy-dispersive X-ray spectroscopy (EDS) in a scanning transmission electron microscopy (STEM) demonstrated the formation of an intermetallic compound,  $\beta\text{-Al}_3\text{Mg}_2$ , in the form of thin layers of  $\approx 20$  nm and  $\approx 30$  nm in the Al matrix after 5 and 10 turns, respectively. An example of the intermetallic nanolayer is shown at the white arrows in Figure 2b for the disk edge after five HPT turns. Thus, the processing synthesizes an intermetallic-based Al metal matrix nanocomposite (MMNC) in the highly deformed region around the peripheries of the disks after HPT. Furthermore, a high-resolution TEM photo for the disk edge after 10 turns is shown in Figure 2d<sup>[13]</sup> and it reveals the formation of another intermetallic compound of  $\gamma\text{-Al}_{12}\text{Mg}_{17}$  in the Al matrix which is in a supersaturated solid solution state after 10 turns due to rapid diffusion of Mg from the fine Mg-rich phases which are visible after five turns of HPT. The formation of  $\gamma\text{-Al}_{12}\text{Mg}_{17}$  was also determined by an X-ray diffraction (XRD) analysis with the Materials Analysis Using Diffraction (MAUD) which is based on a full pattern fitting procedure (Rietveld method).<sup>[13]</sup>

The hardness variations along the disk diameters at the mid-sections of the Al–Mg disks are shown in Figure 3 for 1, 5, and 10 turns where, for comparison purposes, the plot includes the hardness ranges of  $\approx 65$  for Al-1050<sup>[16]</sup> and  $\approx 105$  for the ZK60 alloy<sup>[17]</sup> after HPT for five turns in gray and yellow markers, respectively. The disk after one turn showed hardness values within  $\approx 60$ –100 and the wide variation is due to the measurement locations on different phases of Al or Mg. However, no visible hardness variation was observed along the disk diameter in the multi-layered Al–Mg which is contrary to conventional metals and alloys after HPT for one

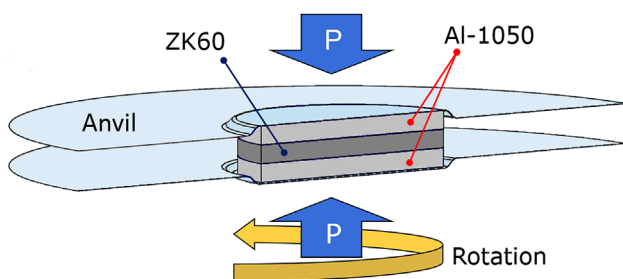


Fig. 1. Schematic illustration of the sample set-up in the HPT facility.

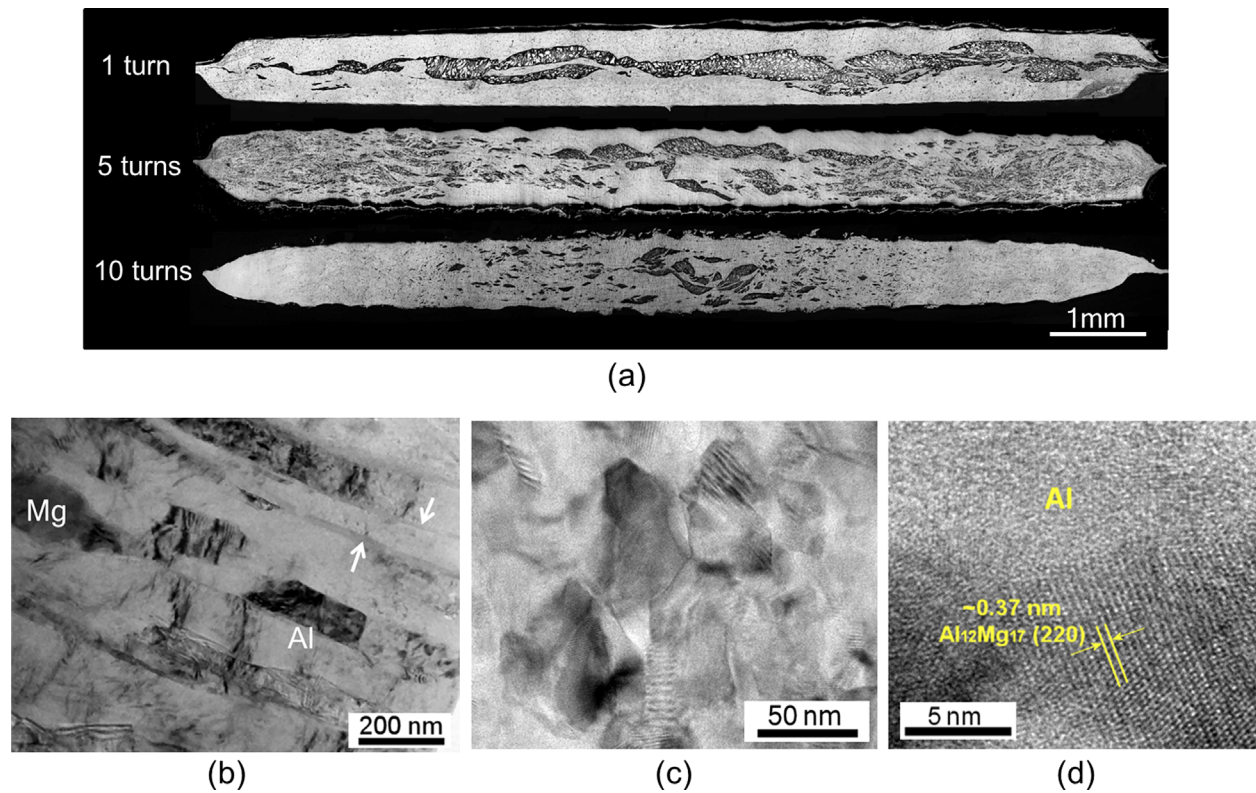


Fig. 2. (a) Vertical cross-sections of the Al–Mg system after HPT for 1, 5, and 10 turns and the observed TEM micrographs for the disk edges of (b) five turns and (c)–(d) 10 turns.<sup>[13]</sup>

turn where a large difference in hardness is generally found from the disk center toward the periphery in the early stage of HPT.<sup>[18]</sup>

After five turns of HPT, there is no apparent increase in hardness at the central region because the multi-layered structure remains almost the same whereas there is an exceptional hardness at  $r > 4$  mm including a maximum value

of  $H_v \approx 135$ . This hardness is larger than the highest attainable hardness of  $\approx 105$ – $110$  for the ZK60 alloy after HPT for five turns and the very high hardness is attributed to the formation of the MMNC in the peripheral region of the disk.<sup>[13]</sup> Moreover, the disk after 10 turns shows an extremely high hardness of  $H_v \approx 270$  at  $r > 3$  mm and this was attributed to a combination of Hall–Petch strengthening, solid solution strengthening, and precipitation hardening. The simultaneous occurrence of these strengthening processes is a consequence of the rapid processing at a relatively low processing temperature which prevents the occurrence of any significant microstructural recovery.<sup>[13]</sup> It is worth noting that a clear visualization of the hardness variations is available in color-coded contour maps presented earlier for vertical cross-sections of the processed disks.<sup>[13]</sup>

For the formation of MMNC by diffusion bonding of Al and Mg through HPT, a key factor is the occurrence of an enhanced atomic diffusion in nanostructured materials. Several recent reports demonstrated experimental evidence of enhanced atomic diffusion in a Cu–Pb alloy<sup>[19]</sup> and pure Ni<sup>[20]</sup> after ECAP and an Al–Cu alloy system after HPT.<sup>[11]</sup> These earlier reports documented fast diffusion in the processed materials which was attributed to the processing conditions including severe hydraulic pressure<sup>[11,13]</sup> and the formation of extra free volumes due to the high population of lattice defects introduced during processing in the nanostructure<sup>[19,20]</sup>

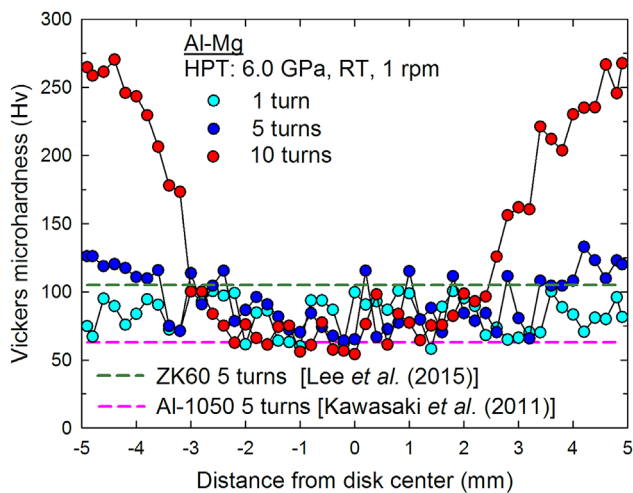


Fig. 3. Hardness variations along the diameters of the Al–Mg disks after HPT for 1, 5, and 10 turns including data for the as-processed alloys of ZK60<sup>[17]</sup> and Al-1050.<sup>[16]</sup>

3. Micro-Mechanical Behavior of the Al–Mg Nanocomposite

The plastic behavior in the Al–Mg multi-layered nanocomposite was examined after HPT for five turns at room temperature using a nanoindentation facility, Nanoindenter-XP (formerly MTS; now Agilent, Oak Ridge, TN) with a three-sided pyramidal Berkovich indenter having a centerline-to-face angle of 65.3°. To provide statistically valid data, more than 15 indentations were conducted at specific phases at the centers and edges of the disks. All measurements by nanoindentation testing were conducted under a predetermined peak applied load of  $P_{max} = 50$  mN at various constant loading rates with  $\dot{\epsilon}_i = h^{-1}(dh/dt)$  of 0.0125, 0.025, 0.05, and 0.1 s<sup>-1</sup> which corresponded to strain rates,  $\dot{\epsilon}$ , of  $1.25 \times 10^{-4}$ ,  $2.5 \times 10^{-4}$ ,  $5.0 \times 10^{-4}$ , and  $1.0 \times 10^{-3}$  s<sup>-1</sup> calculated through an empirical relationship.<sup>[21,22]</sup> Thermal drift was maintained below 0.1 nm s<sup>-1</sup> in all experiments and the data were normalized with the thermal effect during the indentation procedure.

Figure 4 shows representative load–displacement curves for (a) Al and (b) Mg phases at the disk center when measuring at a strain rate of  $1.0 \times 10^{-3}$  s<sup>-1</sup> and for the Al–Mg multi-layered phase at the disk edge when measuring at strain rates of (c)  $1.0 \times 10^{-3}$  s<sup>-1</sup>, (d)  $5.0 \times 10^{-4}$  s<sup>-1</sup>, (e)  $2.5 \times 10^{-4}$  s<sup>-1</sup>, and (f)  $1.25 \times 10^{-4}$  s<sup>-1</sup> after five turns by HPT. It should be noted that the discontinuities of the curves at the final stages

of unloading are due to thermal expansion and these effects can be omitted from the analysis.

A series of indentation curves in Figure 4a and b show less broadening between separate measurements in both the Al and Mg phases, thereby demonstrating consistent mechanical response within the phases in the multi-layered microstructure at the center of the processed disk. It is also apparent from these plots that higher plasticity was achieved in the Al phase compared with the Mg phase in the central region after HPT for five turns. These trends are consistent for different indentation strain rates for the Al and Mg phases at the disk center.

The mechanical behavior in Figure 4c for the disk edge is directly comparable with Figure 4a and b for the disk center due to the consistent indentation testing conditions. Some curves in Figure 4c demonstrating the highest attainable plasticity show reasonably consistent results for the Mg phase at the disk center as shown in Figure 4b and the remaining curves show less plasticity so that there is a wide deviation in plastic behavior, and thus in the plastic instability, at the disk edge. Although it was not possible to identify the exact measurement locations at the disk edge due to the complexity of microstructure after five HPT turns as shown in Figure 2a, the variation in the plastic behavior is due to the existence of the intermetallic compound of  $\beta\text{-Al}_3\text{Mg}_2$  at the peripheral region of the disk after five turns.

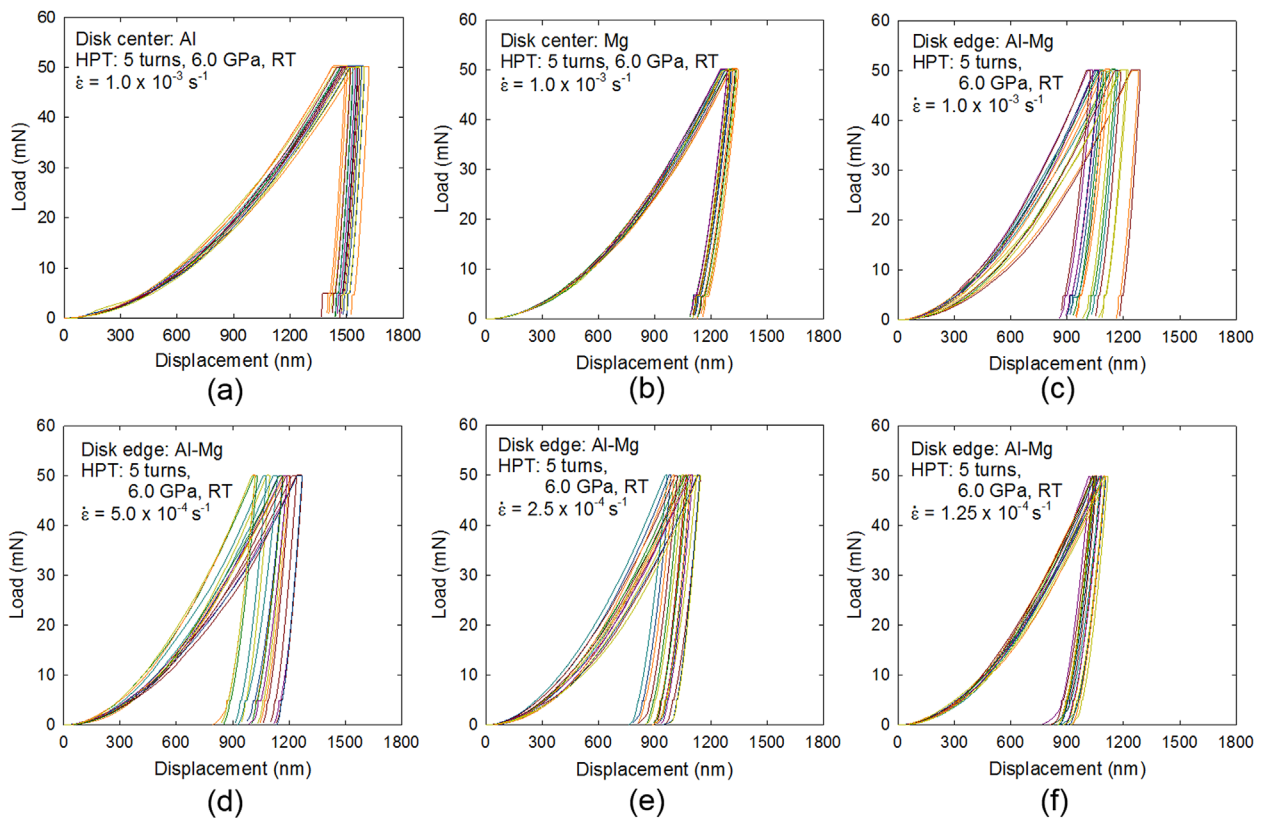


Fig. 4. Representative load–displacement curves for (a) Al and (b) Mg phases at the disk center at a strain rate of  $1.0 \times 10^{-3}$  s<sup>-1</sup> and for the Al–Mg multi-layered phase at the disk edge when testing at (c)  $1.0 \times 10^{-3}$  s<sup>-1</sup>, (d)  $5.0 \times 10^{-4}$  s<sup>-1</sup>, (e)  $2.5 \times 10^{-4}$  s<sup>-1</sup>, and (f)  $1.25 \times 10^{-4}$  s<sup>-1</sup> for the sample after five turns by HPT.

The disk edge after HPT for five turns containing an intermetallic compound, thus forming an MMNC, was tested by nanoindentation at different strain rates and the results are shown in Figure 4c–f. It is apparent that the faster strain rate shows wider broadening within the datum curves under the same testing condition and the broadening within the curves becomes smaller with decreasing indentation strain rate, thereby demonstrating a large plastic instability at higher strain rates in the Al–Mg MMNC in the present testing conditions. However, close inspection indicates that the instability tends to decrease by shifting the curves to the right showing higher plasticity toward the left so that the Al–Mg phase at the peripheral region shows consistently low plasticity after five turns when deformed at low strain rate. The micro-mechanical behavior observed in the MMNC may be compared with conventional metals and alloys where materials generally show a strain rate dependency for the peak load displacement. In practice, faster strain rates lead to smaller indentation displacements and thus lower plasticity and this behavior was shown recently in a Zn–22% Al eutectoid alloy after HPT through four turns.<sup>[23]</sup>

The deformation characteristics at room temperature may be evaluated for the multi-layered structure at the disk center and the MMNC at the disk edge in the Al–Mg alloy after HPT for five turns by calculating the essential material properties of strain rate sensitivity,  $m$ , from the data set of nanoindentation testing shown in Figure 4. Considering Tabor’s empirical prediction where the flow stress is equivalent to  $H/3$  for fully plastic deformation at a constant strain rate,  $\dot{\epsilon}$ ,<sup>[24]</sup> in which  $H$  is the nanoindentation hardness estimated according to the Oliver–Pharr method,<sup>[25]</sup> the value of  $m$  is determined by the expression:<sup>[26]</sup>

$$m = \left( \frac{\partial \ln \sigma_f}{\partial \ln \dot{\epsilon}} \right)_{\epsilon, T} = \left( \frac{\partial \ln(H/3)}{\partial \ln \dot{\epsilon}} \right)_{\epsilon, T} \quad (1)$$

Thus, the value of  $m$  was calculated from the slope of the line for each measurement location in a logarithmic plot of  $H/3$  against  $\dot{\epsilon}$  as shown in Figure 5 for (a) the Al and Mg phases measured at the center and (b) the Al–Mg phase at the edge of the disk after HPT for five turns. It should be noted that the

error bars represent the standard deviation of the numbers of measurements for each condition, as shown in Figure 4.

Figure 5a shows estimated strain rate sensitivities of  $\approx 0.04$  and  $\approx 0.01$  for the Al and Mg phases, respectively, within the multi-layered structure at the disk center after five turns. The  $m$  value for the Al phase shows reasonable agreement with  $\approx 0.03$  obtained by nanoindentation at a mid-diameter of a high-purity Al disk after HPT for five turns<sup>[27]</sup> and also by compression testing on a high-purity Al billet after ECAP for eight passes at room temperature.<sup>[28]</sup> These  $m$  values are typical of an fcc structure deformed at low temperatures.<sup>[29,30]</sup> For the observed  $m$  value for the Mg phase at the disk center, there is a reasonable consistency with earlier reports showing  $m$  values of 0.008–0.015,<sup>[31]</sup> 0.012–0.017,<sup>[32]</sup> and 0.018–0.029<sup>[33]</sup> observed by tensile testing of an AZ31 magnesium alloy after rolling and with the value of 0.016–0.02 observed by tensile testing of an Mg–2.7Zn–0.75Zr–0.45Ag–0.17Ca–0.07Mn alloy after ECAP for eight passes at 498 K.<sup>[34]</sup> By contrast, a recent report showed high  $m$  values of 0.035–0.045 measured by nanoindentation of a ZK60 magnesium alloy after HPT up to two turns.<sup>[35]</sup> Nevertheless, it is reasonable to conclude that the separate phases in the multi-layered structure show similar plastic behavior to the same materials when processed separately by HPT.

The strain rate sensitivity for the Al–Mg MMNC at the disk edge was estimated as  $m \approx 0.01$  taken from the average of  $H/3$ . However, as was apparent in Figure 4c–f, the plastic behavior of the Al–Mg MMNC phase shows a wide plastic instability at the present testing strain rates so that the datum points with error bars in Figure 5b imply the possibility of a much smaller strain rate sensitivity. In practice, deformation behavior with a decreased strain rate sensitivity can explain the micro-mechanical response at the disk edge as shown in Figure 4c–f where the material demonstrates a loss of high plastic characteristics and thus, in general, becomes hard and brittle with decreasing strain rate.

A negative strain rate sensitivity was observed earlier in several coarse-grained Al alloys.<sup>[36–38]</sup> Specifically, the behavior consists of the deformation becoming inhomogeneous and leading to an instability of plasticity and thus to the Portevin–Le Chatelier effect. This is attributed to the occurrence of

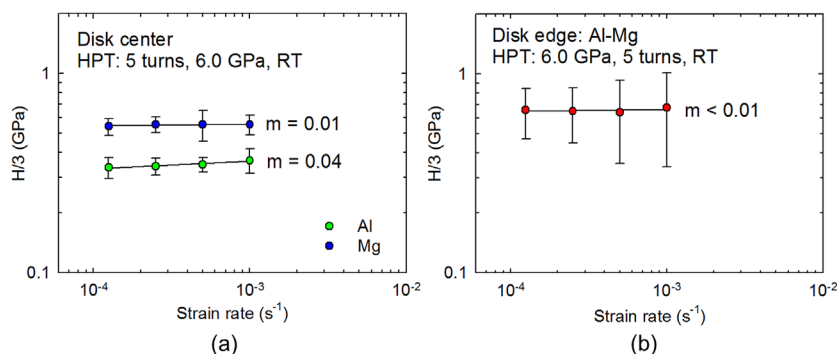


Fig. 5. Variations of the strain rate sensitivity with increasing strain rate for (a) the Al and Mg phases measured at the center and (b) the Al–Mg phase at the edge of the disk after HPT for five turns.

dynamic strain aging (DSA) and demonstrates a host of small-scale phenomena associated with the interactions of dislocations and solute atoms.<sup>[39]</sup> Thereafter, a negative strain rate sensitivity was also observed in nanostructured Ti after ECAP followed by cold rolling<sup>[40]</sup> and in a bulk cryomilled ultrafine-grained Al–7.5% Mg alloy.<sup>[41]</sup> Further investigation of a cryomilled Al–5083 alloy demonstrated that the negative strain rate sensitivities in both nanostructured and coarse-grained Al alloys were caused by DSA.<sup>[42]</sup> Specifically, DSA occurs due to the formation of solute clusters on forest dislocations resulting in a strengthening of dislocation junctions where the presence of a cluster on a forest dislocation modifies the strength of the junction formed by the interaction of dislocations with mobile unclustered dislocations. Thus, faster deformation allows for less clustering by diffusion of solute atoms to the mobile dislocations and this produces junctions having lower strength.<sup>[39,42]</sup> It should be noted that the PLC effect is generally observed over a limited range of temperature and strain rate and thus the testing conditions of room temperature to 50 °C and strain rates of  $<10^{-1} \text{ s}^{-1}$  were suggested for commercial Al alloys demonstrating a negative strain rate sensitivity.<sup>[36]</sup>

An earlier experiment on a discontinuously reinforced metal matrix composite of a powder-consolidated aluminum 6092/B<sub>4</sub>C demonstrated a negative strain rate sensitivity at strain rates  $<1.0 \text{ s}^{-1}$ .<sup>[43]</sup> The report documented the phenomena of DSA due to the presence of the fast diffusion of solute atoms interacting with mobile dislocations. Thus, in the present case of an Al MMNC, since the plastic instability tends to have a strong grain refinement dependence when testing at room temperature<sup>[44]</sup> and a fast atomic diffusivity after HPT,<sup>[13]</sup> a micro-mechanical behavior showing a decreasing strain rate sensitivity is feasible due to the influence of DSA at the disk edge after HPT for five turns under the nano-indentation measurement conditions.

#### 4. Potential for Using HPT in the Development of MMNCs

An earlier study documented a potential for making use of HPT at ambient temperature for the rapid synthesizing of intermetallic-based MMNCs having exceptionally high strength in the Al–Mg system.<sup>[13,14]</sup> The present experiments using nanoindentation testing confirm this approach by describing the plastic behavior of the multi-layered phases at the disk center and at the peripheral region forming the MMNC. Different micro-mechanical responses are observed where the central regions show the characteristics of each specific phase depending on the measured phase whereas the peripheral area demonstrates a decreased strain rate sensitivity by DSA.

In general, a decreased strain rate sensitivity is not desirable when considering the improvement in plasticity of materials during room temperature testing. Considering the similarity in a general trend of plasticity and ductility, this deficiency in plasticity is especially critical for UFG and nanostructured materials where there is usually high strength

but only very limited ductility.<sup>[45–47]</sup> However, behavior with a decreased strain rate sensitivity is controlled by the diffusion activity and the effect of DSA disappears at sufficiently high strain rates for any given testing temperature. Thus, a high strain rate hardening response was observed in nanostructured Ti after ECAP and cold rolling<sup>[40]</sup> and in an aluminum 6092/B<sub>4</sub>C composite through powder consolidation<sup>[43]</sup> both at strain rates  $>10^3 \text{ s}^{-1}$  where these materials demonstrated negative rate sensitivities below  $10^{-3} \text{ s}^{-1}$ . It is noted that the transition from negative to positive strain rate sensitivity occurs between 1 and  $10^3 \text{ s}^{-1}$ .<sup>[43]</sup> Accordingly, although it depends upon the ability for strain hardening of the material, the possibility for attaining high strain rate sensitivity at high strain rates is attractive for achieving high plasticity in UFG and nanostructured materials.

It should be noted that the processed disks of the Al–Mg system contain a variety of microstructures from the multi-layered condition at the disk center to the MMNC at the disk edge after processing through HPT for at least five turns, thereby demonstrating a gradient-type nanostructure in the final bulk solid. This is a new type of structure in engineering materials and recent reports demonstrate an excellent potential for this type of microstructure in exhibiting superior mechanical properties.<sup>[48–51]</sup>

In order to provide a better understanding of the high potential of these unique bulk solids produced by processing dissimilar metals of Al and Mg alloys through the application of HPT, it is instructive to use a toughness–strength diagram reported earlier and delineating the range of fracture toughness and strength-to-weight ratio for many metals and materials.<sup>[52]</sup> The synthesized Al–Mg system after HPT is now incorporated into the diagram and the result is shown in Figure 6 where the region of the HPT-induced aluminum MMNC is shifted to the right and covers a wide area by comparison with the regions for conventional Al and Mg alloys. Since infinite combinations of different Al and Mg alloys are available, the attainable mechanical properties are also reasonably unrestricted and thus the region of the HPT-induced aluminum MMNCs is designated in Figure 6 without delineating any upper limits. It is reasonable to note that the value of  $\approx 350 \text{ MPa cm}^3 \text{ g}^{-1}$  was applied for the border of the strength-to-weight ratio. This is derived from  $H_v \approx 270$  which is equivalent to  $\approx 865 \text{ MPa}$  in tensile strength leading to the excellent strength/weight ratio of  $\approx 350 \text{ MPa cm}^3 \text{ g}^{-1}$  under a measured density of  $2.48 \text{ g cm}^{-3}$  for the disk edge of the present Al–Mg system after HPT for 10 turns.<sup>[13]</sup>

This diagram is proposed with a consideration of the general similarity in the trends of plasticity and toughness of materials<sup>[53]</sup> but it is recognized that more detailed experiments will be required in the future to precisely delineate the limits of this approach. Nevertheless, the present study offers significant opportunities for research in synthesizing future materials using conventional engineering metals. It is concluded that more intensive studies are now needed to confirm the feasibility of making use of HPT for synthesizing other metallic systems containing MMNCs.

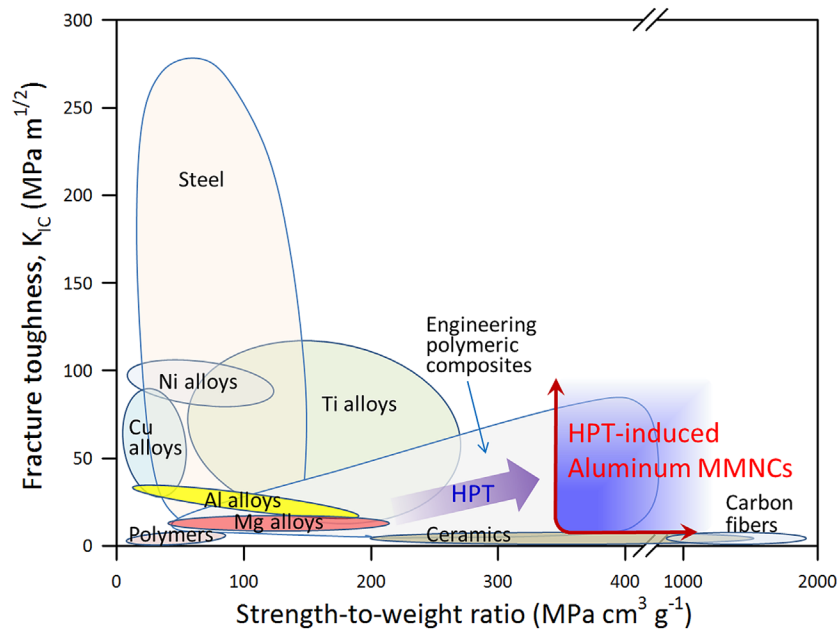


Fig. 6. The range of fracture toughness and strength-to-weight ratio for many metals and materials<sup>[52]</sup> where the synthesized Al–Mg system after HPT is incorporated as the region of HPT-induced aluminum MMNCs without delineating any upper limits.

### 5. Summary and Conclusions

- 1) The present study demonstrates the room temperature micro-mechanical behavior of an Al–Mg alloy system through nanoindentation testing. The material was synthesized by processing separate Al and Mg disks simultaneously through conventional HPT processing for five turns at room temperature under an applied pressure of 6.0 GPa.
- 2) The processed Al–Mg alloy contained a multi-layered structure at the disk center and formed an intermetallic-based metal matrix nanocomposite (MMNC) at the disk edge so that the plastic behavior varied significantly throughout the disk diameter. In practice, the disk center showed mechanical characteristics that were essentially consistent with the initial metals of Al and Mg at the corresponding phases whereas at the disk edge there was significant plastic instability, especially at higher indentation strain rates, with evidence for a decrease in the strain rate sensitivity.
- 3) The processed bulk solid contained a gradient-type nanostructure and, by selecting fast strain rates to avoid dynamic strain aging, it is shown that the Al–Mg alloy system, including the MMNC after HPT, has a significant potential for making use of this approach in future materials. Further investigations are now needed to fully explore the possibility of MMNC synthesis through the use of different engineering metals and alloys.

Article first published online: April 18, 2016

Manuscript Revised: November 17, 2015

Manuscript Received: October 14, 2015

- [1] R. Z. Valiev, R. K. Islamgaliev, I. V. Alexandrov, *Prog. Mater. Sci.* **2000**, *45*, 103.
- [2] A. P. Zhilyaev, T. G. Langdon, *Prog. Mater. Sci.* **2008**, *53*, 893.
- [3] T. G. Langdon, *Acta Mater.* **2013**, *61*, 7035.
- [4] J. M. Cubero-Sesin, Z. Horita, *Mater. Sci. Eng. A* **2012**, *558*, 462.
- [5] K. Kaneko, T. Hata, T. Tokunaga, Z. Horita, *Mater. Trans.* **2009**, *50*, 76.
- [6] K. Edalati, S. Toh, M. Watanabe, Z. Horita, *Scr. Mater.* **2012**, *66*, 386.
- [7] K. Edalati, S. Toh, H. Iwaoka, M. Watanabe, Z. Horita, D. Kashioka, K. Kishida, H. Inui, *Scr. Mater.* **2012**, *67*, 814.
- [8] K. V. Rajulapati, R. O. Scattergood, K. L. Murty, Z. Horita, T. G. Langdon, C. C. Koch, *Metall. Mater. Trans. A* **2008**, *39A*, 2528.
- [9] K. Edalati, S. Toh, H. Iwaoka, Z. Horita, *Acta Mater.* **2012**, *60*, 3885.
- [10] P. Jenei, J. Gubicza, E. Y. Yoon, H. S. Kim, *J. Alloys Compd.* **2012**, *539*, 32.
- [11] K. Oh-ishi, K. Edalati, H. S. Kim, K. Hono, Z. Horita, *Acta Mater.* **2013**, *61*, 3482.
- [12] O. Bouaziz, H. S. Kim, Y. Estrin, *Adv. Eng. Mater.* **2013**, *15*, 336.
- [13] B. Ahn, A. P. Zhilyaev, H.-J. Lee, M. Kawasaki, T. G. Langdon, *Mater. Sci. Eng. A* **2015**, *635*, 109.
- [14] M. Kawasaki, B. Ahn, H.-J. Lee, A. P. Zhilyaev, T. G. Langdon, *J. Mater. Res.* **2016**, *31*, 88.
- [15] R. B. Figueiredo, P. R. Cetlin, T. G. Langdon, *Mater. Sci. Eng. A* **2011**, *528*, 8198.

- [16] M. Kawasaki, S. N. Alhajeri, C. Xu, T. G. Langdon, *Mater. Sci. Eng. A* **2011**, 529, 345.
- [17] H.-J. Lee, S. K. Lee, K. H. Jung, G. A. Lee, B. Ahn, M. Kawasaki, T. G. Langdon, *Mater. Sci. Eng. A* **2015**, 630, 90.
- [18] M. Kawasaki, *J. Mater. Sci.* **2014**, 49, 18.
- [19] S. V. Divinski, J. Ribbe, D. Baither, G. Schmitz, G. Reglitz, H. Rösner, K. Sato, Y. Estrin, G. Wilde, *Acta Mater.* **2009**, 57, 5706.
- [20] S. V. Divinski, G. Reglitz, H. Rösner, Y. Estrin, G. Wilde, *Acta Mater.* **2011**, 59, 1974.
- [21] C. L. Wang, Y. H. Lai, J. C. Huang, T. G. Nieh, *Scr. Mater.* **2010**, 62, 175.
- [22] I.-C. Choi, B.-G. Yoo, Y.-J. Kim, M.-Y. Seok, Y. M. Wang, J.-I. Jang, *Scr. Mater.* **2011**, 65, 300.
- [23] I.-C. Choi, Y.-J. Kim, B. Ahn, M. Kawasaki, T. G. Langdon, J.-I. Jang, *Scr. Mater.* **2014**, 75, 102.
- [24] S. Shim, J.-I. Jang, G. M. Pharr, *Acta Mater.* **2008**, 56, 3824.
- [25] W. C. Oliver, G. M. Pharr, *J. Mater. Res.* **1992**, 7, 1564.
- [26] I.-C. Choi, Y.-J. Kim, Y. M. Wang, U. Ramamurty, J.-I. Jang, *Acta Mater.* **2013**, 61, 7313.
- [27] N. Q. Chinh, T. Csanádi, T. Györi, R. Z. Valiev, B. B. Straumal, M. Kawasaki, T. G. Langdon, *Mater. Sci. Eng. A* **2012**, 543, 117.
- [28] N. Q. Chinh, P. Szommer, T. Csanádi, T. G. Langdon, *Mater. Sci. Eng. A* **2006**, 434, 326.
- [29] H. S. Kim, Y. Estrin, *Appl. Phys. Lett.* **2001**, 79, 4115.
- [30] J. Chen, Y. N. Shi, K. Lu, *J. Mater. Res.* **2005**, 20, 2955.
- [31] A. S. Khan, A. Pandey, T. Gnäupel-Herold, R. K. Mishra, *Int. J. Plast.* **2011**, 27, 688.
- [32] W. J. Kim, H. W. Lee, S. J. Yoo, Y. B. Park, *Mater. Sci. Eng. A* **2011**, 528, 874.
- [33] Q. Yang, A. K. Ghosh, *Acta Mater.* **2006**, 54, 5159.
- [34] F. H. Dalla Torre, A. C. Hänzi, P. J. Uggowitzer, *Scr. Mater.* **2008**, 59, 207.
- [35] I.-C. Choi, D.-H. Lee, B. Ahn, K. Durst, M. Kawasaki, T. G. Langdon, J.-I. Jang, *Scr. Mater.* **2015**, 94, 44.
- [36] J. C. Huang, G. T. Gray, *Scr. Metall. Mater.* **1990**, 24, 85.
- [37] J. C. Balík, P. Lukáč, *Acta Metall. Mater.* **1993**, 41, 1447.
- [38] R. C. Picu, G. Vincze, F. Ozturk, J. J. Gracio, F. Barlat, A. M. Maniatty, *Mater. Sci. Eng. A* **2005**, 390, 334.
- [39] R. C. Picu, *Acta Mater.* **2004**, 52, 3447.
- [40] D. Jia, Y. M. Wang, K. T. Ramesh, E. Ma, Y. T. Zhu, R. Z. Valiev, *Appl. Phys. Lett.* **2001**, 79, 611.
- [41] B. Q. Han, Z. Lee, S. R. Nutt, E. J. Lavernia, F. A. Mohamed, *Metall. Mater. Trans. A* **2003**, 34A, 603.
- [42] B. Q. Han, J. Huang, Y. T. Zhu, E. J. Lavernia, *Adv. Eng. Mater.* **2006**, 8, 945.
- [43] H. Zhang, K. T. Ramesh, E. S. C. Chin, *Mater. Sci. Eng. A* **2004**, 384, 26.
- [44] M. Wagenhofer, M. A. Erickson-Natishan, R. W. Armstrong, F. J. Zerilli, *Scr. Mater.* **1999**, 41, 1177.
- [45] R. Z. Valiev, I. V. Alexandrov, Y. T. Zhu, T. C. Lowe, *J. Mater. Res.* **2002**, 17, 5.
- [46] R. Valiev, *Nature* **2002**, 419, 887.
- [47] R. Valiev, *Nat. Mater.* **2004**, 3, 511.
- [48] T. H. Fang, W. L. Li, N. R. Tao, K. Lu, *Science* **2011**, 331, 1587.
- [49] X. L. Wu, P. Jiang, L. Chen, J. F. Zhang, F. P. Yuan, Y. T. Zhu, *Mater. Res. Lett.* **2014**, 2, 185.
- [50] X. L. Wu, P. Jiang, L. Chen, F. Yuan, Y. T. Zhu, *Proc. Natl. Acad. Sci. USA* **2014**, 111, 7197.
- [51] K. Lu, *Science* **2014**, 345, 1455.
- [52] K. Lu, *Science* **2010**, 328, 319.
- [53] M. F. Ashby, *Materials Selection in Mechanical Design*, 3rd edition, Butterworth-Heinemann, Oxford, UK **2005**.